MASSACHUSETTS INSTITUTE OF TECHNOLOGY

LINCOLN LABORATORY

A COMPARISON BETWEEN MONOSTATIC AND BISTATIC SCATTERING FROM RAIN AND THIN TURBULENT LAYERS

R. K. CRANE

Group 61

TECHNICAL NOTE 1970-29

6 OCTOBER 1970

LEXINGTON MASSACHUSETTS

The work reported in this document was performed at Lincoln Laboratory, a center for research operated by Massachusetts Institute of Technology. This work was sponsored by the National Aeronautics and Space Administration under Contract NAS 5-21532.

ERRATA SHEET

for

TECHNICAL NOTE 1970-29

The author has detected the following errors in Technical Note 1970-29 (R. K. Crane, "A Comparison Between Monostatic and Bistatic Scattering from Rain and Thin Turbulent Layers [U]," 6 October 1970). Kindly insert these pages into your copy of that report.

Page 5 In the first equation, the upper limits for the integrals in the exponential function should be changed to x_1 and $r_2(x_1)$ as

$$\left[\int_0^{x_1} \beta_E \, dx_1 + \int_0^{r_2(x_1)} \beta_E \, dx_2\right].$$

Page 9 After description of ψ_2 add

$\psi_1 + \psi_2$ = scattering angle.

Page 10 Equation in the middle of the page should be changed to

$$D = \frac{\Delta h}{\sin(\zeta)}$$

and add under where

ζ is the angle between the direction of propagation from antenna 1 to the scatterer at the scatterer and the intersection of the great circle plane of antenna 1 and the scatterer and the local

horizontal surface at the scatterer. For scattering in or near the great circle plane of transmitter and receiver, $\zeta \cong \psi_1$.

Change − to + in exponent of Z in equation at the bottom of the page.

Page 11 Equation (9) should have a $f^{2.7}$ in the denominator. The exponent of Z should be written as $Z^{0.2}$. This equation may also be expressed as

$$\frac{1}{L} = \frac{G_2(\hat{r}_2) C_p \xi Z^{0.2} \lambda^{0.7}}{r_2^2} \left(1 - e^{-3.3 \times 10^{-6} \lambda^{-2.7} Z^{0.8} D}\right)_{(1.8 \times 10^{-12})} .$$

In Eq. (10) replace $\sin \psi_1$ by $\sin \zeta$ in the denominator.

Page 12 Equation (13) replace $\sin \psi_1$ by $\sin \zeta$ in the denominator.

Page 32 Fourth line from the bottom, replace Fig. 13 by Fig. 14.

Page 38 In the last line, replace Fig. 14 by Fig. 13 and Fig. 13 by Fig. 12.

Publications
M. I. T., Lincoln Laboratory
P. O. Box 73
Lexington, Massachusetts 02173

25 January 1971

ABSTRACT

Simultaneous measurements were made of the backscatter cross section and the bistatic scattering cross section of rain and thin turbulent layers. The radar measurements were made at a frequency of 1.3 GHz using the Millstone Hill Radar. The bistatic scattering measurements were made using CW transmission at 7.7 GHz with a 145-km separation between transmitter and receiver. The receive station was the Westford Communication Terminal with a 60-foot antenna. The transmitter was van-mounted and used either a 6-foot antenna or a standard gain horn. Stable frequency sources were used to allow doppler shift measurements on the bistatic scattering link. The measurements were made by fixing the pointing angles of the transmit antenna and scanning both the receive antenna and the radar to investigate the dependence of the scattered signals both on scattering angle and on the location of the scatterers.

The measurements of the scattering cross section of the thin turbulent layers were made in the near forward direction, the measurements of rain at a large number of scattering angles. System sensitivities allowed the measurement of scattering from turbulent layers at a 10-km height with a thickness, C_n^2 product of $10^{-13} N^2 m^{1/3}$ and from rain with a 0.1 mm/hr. rate. Comparisons between the radar and bistatic measurements were in good agreement with the appropriate scattering theories.

CONTENTS

A Comparison Between Monostatic and Bistatic Scattering from Rain and Thin Turbulent Layers

I. INTRODUCTION

Current and proposed frequency allocations allow for the sharing of bands in the microwave region between satellite communication and terrestrial communication services. The extent to which the bands may be shared depends upon possible interference between systems that operate at the same frequency but for different services. The prediction of interference between two systems operating at the same frequency and beyond each others radio horizon requires the prediction of high level fields caused by one of the several mechanisms for transhorizon propagation. Four basic transhorizon propagation mechanisms may be identified, scattering by rain, scattering by thin turbulent layers, terrain diffraction, and ducting. The prediction of interference due to any of these mechanisms requires a model for the computation of field strength given the appropriate meteorological parameters and the statistics of those parameters.

This technical note is addressed to the models required for the computations of field strength given the appropriate meteorological parameters. For the two mechanisms receiving the most attenuation, rain and turbulent layer scattering, the meteorological parameter selected is the radar scattering cross section per unit volume which may be measured by a weather radar. This is not a parameter for which an adequate climatological description is

available. The lack of an adequate climatological description limits the utility of the models for the direct prediction of the statistics of interference. This parameter was selected because it provides the best description of the physical processes involved, its extreme values may be estimated from available data, and the problem of using other available climatological data for the prediction of its statistics is being worked on. No meteorological parameters were selected for the other two mechanisms because their effects will be mitigated with adequate site shielding.

The models developed for rain and thin turbulent layer scattering have been simplified so that they directly relate the transmission loss to the antenna parameters and pointing angles, the intensity of the scattering phenomena, and the "half width" of the scattering phenomena. The models were verified by measurements made at X-band on a 145-km scatter path between Avon, Connecticut, and the Westford Communications Terminal and at L-band with the Millstone Hill Radar located approximately 0.5 km from the Communications Terminal. The data showed agreement between the transmission loss obtained from the scatter-path measurements and the estimated transmission loss based upon model computations and the simultaneous radar measurements. The measurements also show that both foliage and solid earth shielding will increase the transmission loss.

II. SCATTER MODELS

Scattering from both rain and thin turbulent layers may be modeled as

scattering from a distribution of volume scatterers. The per unit volume scattering cross sections may be obtained from the appropriate scattering theory and the effective scattering volume from the antenna patterns and a physical description of the scattering phenomena. Using the per unit volume scattering cross section and the bistatic radar equation, the transmission loss between two antennas beyond each others radio horizon is given by

$$\frac{P_r}{P_t} = \frac{1}{L} = \frac{G_1 G_2 \lambda^2}{(4\pi)^3} \int_{vol} \frac{C_p g_1 g_2 \beta_s}{r_1^2 r_2^2} e^{-\left[\int_0^{r_1} \beta_E dx_1 + \int_0^{r_2} \beta_E dx_2\right]} d\,vol \quad (1)$$

where P_r = received power

P_t = transmitted power

L = transmission loss

λ = wavelength

G_1, G_2 = antenna gain for antennas 1 and 2, respectively

g_1, g_2 = antenna gain function

C_p = polarization loss

β_s = scattering cross section per unit volume for the elemental integration volume d vol

β_E = extinction cross section per unit volume at the location of dx

$= \frac{A}{4.34}$ where A = attenuation per unit length

dx_1, dx_2 = elemental length along the ray from the antenna to the elemental integration volume

r_1, r_2 = distance along the ray from the antenna to the elemental integration volume.

The bistatic radar equation, Eq. (1), assumes that the scattering process may be described by single scattering theory and that the scattering and extinction cross sections are known throughout space. From previous weather radar measurements (Crane, 1968a and 1968b) it is known that the scatterers are not uniformly distributed throughout space. The important turbulent scatterers are confined to thin turbulent layers with a scattering cross section at least a factor of 2 greater than that for the surrounding volume. The important rain scatterers are confined in small cells with scattering cross sections at least an order of magnitude greater than that for the rain in the surrounding mesoscale areas. As an approximation, it will be assumed that the layer or cell fills one of the antenna beams, the antenna beam with the smaller cross section or $r\varphi$ product where φ is the antenna half-power beamwidth and r is the distance from the antenna to the scatterers. Letting the subscript 1 refer to the antenna with the smaller $r\varphi$ product, assuming that the effective scattering volume is defined by the antenna pattern and the distance occupied by the scattering layer or cell along the antenna beam, and assuming that the scattering volume is small enough for C_p, r_1 and r_2 to be a constant, Eq. (1) may be written as

$$\frac{1}{L} = \frac{G_1 G_2 \lambda^2 C_p}{(4\pi)^3 r_1^2 r_2^2} \int g_1 g_2 \beta_s \, e^{-\left[\int_0^{r_1} \beta_E \, dx_1 + \int_0^{r_2} \beta_E \, dx_2\right]} d\,vol \quad .$$

This equation may be further simplified by assuming that the beamwidth of antenna 1 is small enough for β_s to be constant over angular volume coordinates within the beam, that the other beamwidth is sufficiently large for the scattering volume to limit the range integration from antenna 1, and that the gain of antenna 2 is constant over the effective integration volume. With these approximations, Eq. (1) becomes

$$\frac{1}{L} = \frac{G_1 G_2 g_2 C_p \beta_s \lambda^2}{(4\pi)^3 r_1^2 r_2^2} \int_0^{4\pi} \int_0^{\infty} g_1(\Omega_1) S(x_1) e^{-\left[\int_0^{r_1} \beta_E dx_1 + \int_0^{r_1} \beta_E dx_2\right]} dx_1 r_1^2 d\Omega_1$$

where $S(\mathbf{x})$ describes the change in scattering cross section with distance along the ray from antenna 1.

To readily evaluate the integral, further assumptions must be made about the effect of attenuation. The attenuation phenomena will be split into two parts, one that represents attenuation due to all regions outside the cell or layer and one that describes the attenuation within. The attenuation within the scattering volume will also be assumed to have some functional dependence upon x_1. With these assumptions, Eq. (1) becomes

$$\frac{1}{L} = \frac{G_1 G_2 g_2 \lambda^2 C_p \beta_s \xi}{(4\pi)^3 r_2^2} \int_0^{4\pi} g_1(\Omega_1) d\Omega_1 \int_0^{\infty} S(x_1) e^{-\beta_E \int_0^{x_1} \left[\mu_1(x) + \mu_2(x)\right] dx} dx_1 d\Omega_1 \quad (2)$$

where $\xi = e^{-\left[\int_0^{r_1} \beta_E dx_1 + \int_0^{r_2} \beta_E dx_2\right]}$

$\mu_1(x)$ describes the dependence of the attenuation coefficient on distance along the ray within the scattering volume.

$\mu_2(x)$ describes the attenuation between the edge of the volume and point x_1 along the ray from antenna 2.

The μ_1, μ_2 functions are readily determined for two cases, small angle forward scatter for which

$$\int_0^{x_1} \left[\mu_1(x) + \mu_2(x)\right] dx = \int_0^{\infty} S^{\gamma}(x)\, dx$$

where the functional relationship $\beta_E \propto \beta_s^{\gamma}$ has been assumed and backscattering for which

$$\int_0^{x_1} \left[\mu_1(x) + \mu_2(x)\right] dx = 2 \int_0^{x_1} S^{\gamma}(x)\, dx \quad .$$

The integrals may now be evaluated when models are chosen for $g_1(\Omega_1)$ and for S(x). The simplest model assumes that the antenna detects no signal for angles greater than $\varphi/2$ and has a unity gain function for angles less than $\varphi/2$ and that S(x) is unity within a volume of length D along the antenna beam and zero outside. With these assumptions the integrals become

$$\Lambda_F = \int_0^{4\pi} g_1(\Omega_1) \int_0^{\infty} S(x_1)\, e^{-\beta_E \int_0^{\infty} S^{\gamma}(x)\, dx}\, dx_1$$

$$= \frac{\pi \varphi_1^2 D}{4} e^{-\beta_E D} \qquad \text{near forward scatter}$$

$$\Lambda_B = \frac{\pi \varphi_1^2}{4} \left(\frac{1 - e^{-2\beta_E D}}{2\beta_E} \right) \qquad \text{near backscatter}$$

and

$$\frac{1}{L} = \frac{G_1 G_2 g_2 \lambda^2 C_p \beta_s \Lambda \xi}{(4\pi)^3 r_2^2} \tag{3}$$

with $\Lambda = \Lambda_F$ or Λ_B depending upon the case considered. An improved model may also be constructed by assuming that antenna 1 has a Gaussian antenna pattern and that the scatterers have a Gaussian distribution along the antenna beam.

$$\Lambda_F' = 1.54 \frac{\pi \varphi_2^2}{4} D \, e^{\frac{1.06}{\sqrt{\gamma}} \beta_E D}$$

where D is the distance between the 3 dB down scatterer intensity values along the antenna beam.

Equation (3) may be further simplified by using the relationship between antenna gain and the half-power beamwidth.

$$G_1 = \frac{4\pi \eta \, \text{Area}}{\lambda^2} = \pi^2 \eta \frac{d^2}{\lambda^2} = \frac{\pi^2 \eta C_\varphi^2}{\varphi_1^2}$$

where Area = aperture area of antenna 1

d = diameter of the aperture (assumed circular)

$\varphi = C_\varphi \frac{\lambda}{d}$.

Equation (3) reduces to

$$\frac{1}{L} = \frac{G_2(\hat{r}_2)\, C_p\, \eta\, C_\varphi^2\, \xi\, \lambda^2\, \beta_s\, \Lambda}{(64\pi)\, r_2^2\, \varphi_1^2} \tag{4}$$

where

$G_2(\hat{r}_2) = G_2 g_2$ = gain of antenna 2 in the direction $\hat{r}_2$.

For application to rain or thin turbulent layer scattering, the bistatic scattering cross section per unit volume must be related to the relevant meteorological parameters. For rain, the standard parameter is Z, the sum of the sixth powers of diameters of all the drops in a unit volume (Crane, 1966).

$$\beta_\perp = \frac{\pi^5}{\lambda^4} Z\, |K|^2\, \alpha_\perp(\psi_1 + \psi_2)$$

$$\beta_{||} = \frac{\pi^5}{\lambda^4} Z\, |K|^2\, \alpha_{||}(\psi_1 + \psi_2)$$

where

$\beta_\perp$ is the scattering cross section per unit volume for polarization perpendicular to the plane of scattering.

$\beta_{||}$ is for polarization in the plane of scattering.

$|K|^2$ is a parameter which depends upon the dielectric properties of the raindrops and is near unity for frequencies between 1 and 35 GHz.

$\alpha_\perp, \alpha_{||}$ are factors required to produce equality and depend upon the scattering model used. $\alpha_\perp = \alpha_{||} = 1$ for isotropic scatterers, $\alpha_\perp = 1$, $\alpha_{||} = \cos^2(\psi_1 + \psi_2)$ for Rayleigh scatterers, and for Mie scatterers the factors must be computed for each frequency, drop temperature, and drop-size distribution.

ψ_1 is the angle between the direction of propagation from antenna 1 to the scatterer at the scatterer and the intersection of the plane of scattering and the local horizontal surface at the scatterer.

ψ_2 is the angle between the direction of propagation from the scatterer to antenna 2 and the intersection between the plane of scattering and the local horizontal surface.

For the application of Eq. (4) to rain scattering, the distance D or the rain cell"half width"must also be known. Given Z, D, the antenna parameters, and the scatter-path geometry, the transmission loss for rain scattering may be determined. The model as developed applies to spherical liquid water scatterers and closely approximates rain. For melting snow or hail, the $|K|^2$, $\alpha_\perp$, and $\alpha_{||}$ values must be modified. Both hail and melting snow are large scatterers that have a large forward to back-scattering ratio. Using either the isotropic or Rayleigh scattering model, the field in the near forward scatter direction may be underestimated by as much as 5-10 dB. A better approximation for either the hail or melting snow problem is not available due to a lack of data on particle shapes, dielectric constants, and size distributions.

For thin layer turbulence, the scattering cross section per unit volume is related to C_n^2, a meteorological parameter that describes the intensity of the random fluctuations in the index of refraction for scale sizes in the inertial subrange or roughly 0.01 to 10 meters (Tatarski, 1961). The relationship is given by

$$\beta_\perp = 0.378\lambda^{-1/3} C_n^2 \left[\sin\left(\frac{\psi_1 + \psi_2}{2}\right)\right]^{-11/3}$$

$$\beta_{||} = \beta_\perp \cos^2(\psi_1 + \psi_2) \quad . \tag{6}$$

This expression may be used as long as the scale size, ℓ, selected by the geometry of the scatter path and the operating wavelength is in the inertial subrange

$$.01 \leq \ell = \frac{\lambda}{2 \sin\left(\frac{\psi_1 + \psi_2}{2}\right)} \leq 10, \quad \ell, \lambda \text{ in meters.}$$

This limits the frequencies for use of the thin turbulent layer scattering model to those above 3 GHz. Since the thin layer scattering volume is nearly horizontal,

$$D = \frac{\Delta h}{\sin \psi_1}$$

where Δh is the thin layer thickness or "half width."

Except for a discussion of the effects of attenuation in the scattering volume, the scattering models are complete. In the case of thin layer turbulent scattering, $\beta_E = 0$. For rain, $\beta_E \sim 0$ for frequencies below 5 GHz and may be approximately related to Z for frequencies between 5 and 20 GHz. Above 20 GHz, the simple single scattering model is no longer valid and the models discussed here for rain scattering do not strictly apply. For frequencies between 5 and 20 GHz the attenuation may be related to Z by (based upon Mie theory computations and regression analysis using a large number of drop-size distributions)

$$A = \nu Z^{-\gamma}$$

where

$\gamma \simeq 0.8$

$\nu = 2.4 \times 10^{-7} f^{2.7}$

f = frequency in GHz

Z = is in mm^6/m^3

and A is in dB/km.

Using the above approximations and for the simplest possible model, assuming that $\eta = .5$, $C_\varphi^2 = 1$, $|K|^2 = 1$ and the scattering is isotropic, the following results are obtained:

Rain scatter model, all directions $0 < f < 5$ GHz:

$$\frac{1}{L} = \frac{G_2(\hat{r}_2)\, C_p\, \xi\, Z\, D}{r_2^2 \lambda^2} (6 \times 10^{-18}) \tag{7}$$

Rain scatter model, near forward direction $5 \leq f \leq 20$ GHz:

$$\frac{1}{L} = \frac{G_2(\hat{r}_2)\, C_p\, \xi\, Z\, D}{r_2^2 \lambda^2} e^{-5.5 \times 10^{-8} f^{2.7} Z^{0.8} D} (6 \times 10^{-18}) \quad . \tag{8}$$

Rain scatter model, near backward direction $5 \leq f \leq 20$ GHz:

$$\frac{1}{L} = \frac{G_2(\hat{r}_2)\, C_p\, \xi\, Z^2}{r_2^2 \lambda^2} \left(1 - e^{-1.1 \times 10^{-7} f^{2.7} Z^{0.8} D}\right) (5.5 \times 10^{-11}) \tag{9}$$

Turbulent scatter model, all directions $3 \leq f$ GHz

$$\frac{1}{L} = \frac{G_2(\hat{r}_2)\, C_p\, \xi\, C_n^2\, \Delta h \left[\sin\left(\frac{\psi_1 + \psi_2}{2}\right)\right]^{-11/3}}{r_2^2 \sin \psi_1} \lambda^{5/3} (3.4 \times 10^{-13}) \tag{10}$$

where λ is in cm, r_2 in km, Δh in m, D in km, Z in mm^6/m^3, and C_n^2 in $N^2 m^{-2/3}$. An improved model for near forward scatter may be generated using A'_F and the constants for the particular antenna system as:

Improved rain model, near forward scatter, $0 \leq f \leq 5$ GHz:

$$\frac{1}{L} = \frac{G_2(\hat{r}_2)\, C_p\, \xi\, Z\, D\, \eta\, C_\varphi^2\, |K|^2\alpha}{r_2^2\, \lambda^2} (1.9 \times 10^{-17}) \tag{11}$$

Improved rain model, near forward scatter, $5 \leq f \leq 20$ GHz:

$$\frac{1}{L} = \frac{G_2(\hat{r}_2)\, C_p\, \xi\, Z\, D\, \eta\, C_\varphi^2\, |K|^2\alpha}{r_2^2\, \lambda^2}\, e^{-6.5 \times 10^{-8} f^{2.7} Z^{0.8}} (1.9 \times 10^{-17}) \tag{12}$$

Improved turbulent scatter model, $3 \leq f$ Ghz:

$$\frac{1}{L} = \frac{G_2(\hat{r}_2)\, \xi\, C_n^2\, \Delta h \left[\sin\left(\frac{\psi_1 + \psi_2}{2}\right)\right]^{-11/3} C_p \lambda^{5/3}\, \eta\, C_\varphi^2\, (10^{-12})}{r_2^2 \sin \psi_1} \tag{13}$$

where $\alpha = \alpha_\perp$, $\alpha_\parallel$, or a combination of $\alpha_\perp$ and $\alpha_\parallel$ depending upon the polarization.

The equations (7-13) provide the scattering models for transhorizon propagation due to rain and thin turbulent layers for use in interference prediction and coordination distance computations. Their derivation is predicated on the observation that meteorological scatters are not uniformly distributed in space. The non-uniformity of the scattering volume was used to provide approximate values for the required integrals. The transmission loss values

redicted using these equations are the minimum loss values for the case where antenna 1 points at the scatter volume. The predictions therefore are for cases of main lobe to main lobe, side lobe to main lobe, or main lobe to side lobe coupling. These cases are the significant ones for interference prediction. If, however, an estimate of side lobe, side lobe coupling is desired, a crude model would use the transmission loss for the antenna 1 pointing angle that maximizes the received signal and multiplying the result by the main lobe, side lobe ratio for the angle between the actual pointing direction of antenna 1 and the pointing angle for maximum signal. A second model for side lobe, side lobe coupling that could be used for rain would use the rain cell to define the effective scattering volume, $r_1^2 \Lambda_c = D^2 H$ where H is the height of the cell above the intersection of the cell and the higher of the horizon rays from the antennas.

III. RADAR MEASUREMENTS

Measurements of Z and $C_n^2 \Delta h$ were made with the Millstone Hill L-band Radar for use with the model equations in predicting transmission loss for the Avon to Westford scatter path. The parameters of the radar system are listed in Table I. The radar system was calibrated using satellites with known radar cross sections. The effective integration volume of the radar for measurements of distributed targets was calculated from the measured antenna patterns and pulse shape and is 1.1 km in height, 1.1 km in horizontal distance normal to the plane of the radar and the scattering volume, and

TABLE I

PARAMETERS OF THE MILLSTONE HILL L-BAND RADAR

Frequency	1, 295 GHz (23, 2 cm wavelength)
Antenna	84-foot parabola with Cassegrain feed
Antenna gain	47, 1 dB
Beamwidth	0, 6° between half-power points
Polarization	Right-hand circular transmitted Left-hand circular received
Transmitted power	4 Mw peak (continuously monitored)
Pulse length	10μ sec
Pulse repitition rate	20 per second
Receiver bandwidth	80, 5 Khz (12, 4μ sec matched predetection filter)
Data processing	Analog to digital conversion of IF sine and cosine channels every 10μ sec
Detection	Square Law by computer operation
System noise temperature	280°K (includes atmospheric and ground effects averaged over 0-30° elevation angle)
Overall system feed and line losses	1, 7 dB
Matched filter processing loss	1, 4 dB
Single pulse C_n^2 value for unity signal-to-noise ratio	2×10^{-16} Nm^{2} $^{-2/3}$ at 100 km
Minimum detectable layer C_n^2 value with horizontal averaging and average-noise subtraction	1×10^{-16} Nm^{2} $^{-2/3}$ at 100 km
Single pulse Z value for unity signal-to-noise ratio	1×10^{-3} mm^6/m^3 at 100 km

1.5 km in horizontal distances in the plane of the radar and scattering volume for targets below a 20-km height at a range of 100 km. The effective resolution distance of the radar normal to the antenna beam at 100 km is 1.8 km, the distance between the 10 dB down points on the one-way antenna pattern. For a uniform distribution of scatterers within the radar integration volume, the uncertainty in the calibration of the radar is 1 dB.

Measurements of Z were made by slowly scanning the antenna in azimuth at fixed elevation angles to provide near horizontal maps of rain intensity. The radar incoherently integrated 50 pulses for every range, azimuth resolution cell. During the 50-pulse integration period, the antenna was moved less than a half-power beamwidth in azimuth. Using the statistics of rain scatterers, the cross section estimate for the 50-pulse incoherent average has an rms error of 0.6 dB. A radar map of Z for 7 August 1968 is shown in Fig. 1. In this map, the data is presented as contours of Z in 5 dB steps with the peak values for three cells added. The rain rate estimates were made using the approximate $Z = 200\ R^{1.6}$ relationship. The data used in preparing the map were processed in 0.5 x 3 km resolution cells. The data show the tendency for rain to be distributed in small cells with peak values an order of magnitude higher than that for the surrounding areas.

Measurements of C_n^2 were made by slowly scanning the antenna in elevation over a .2 to 20° elevation angle sector. The scan rate was selected so that the 50-pulse average would be performed with the antenna moving less than

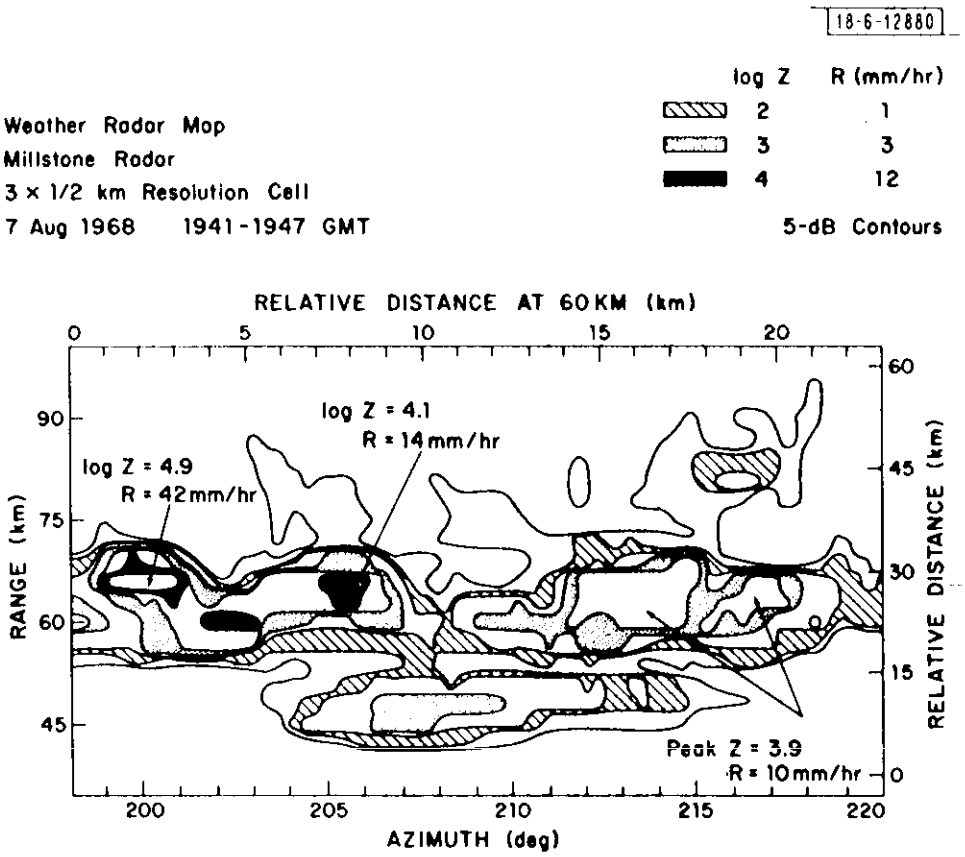

Fig. 1. Weather radar measurements of rain intensity.

a beamwidth. Profiles of C_n^2 were prepared by converting the cross section values as a function of elevation and range to values as a function of surface distance and height and averaging the cross sections at a given height over 22.5 km surface distance intervals. Three horizontal integration intervals were used, 81.1 - 103.6, 104.5 - 127.0 and 128.0 - 150.5 km from the radar. The results for two elevation scans at the same azimuth are presented in Fig. 2. The solid line is for the integration interval closest to the radar, the dashed for the next one out and the dot - dashed for the farthest from the radar. Thin turbulent layers are shown at heights up to 14 km. Due to the limited resolution volume, the layer structure below 4 km is not resolved. With a single frequency radar facility, it is not possible to positively establish whether the layers are caused by refractive index fluctuations or by clouds. The identification must be made by other means. The cirrus layer at 9-km height was identified using weather observer reports and data from simultaneous radiosonde measurements. The identification of the layers below 5 km as being caused by turbulence was made using the simultaneous bistatic scattering data. The C_n^2 values given on Fig. 2 were calculated assuming the layer filled the antenna beam. Aircraft measurements of turbulence often show the layers to be the order of 100 m thick (Crane, 1970). For thin layers, the C_n^2 values would be larger than reported. The $C_n^2 \Delta h$ product is, however, the same when the radar height integration distance, 1.1 km at 100 km, is used for Δh. Since the $C_n^2 \Delta h$ value is required for the estimation of bistatic

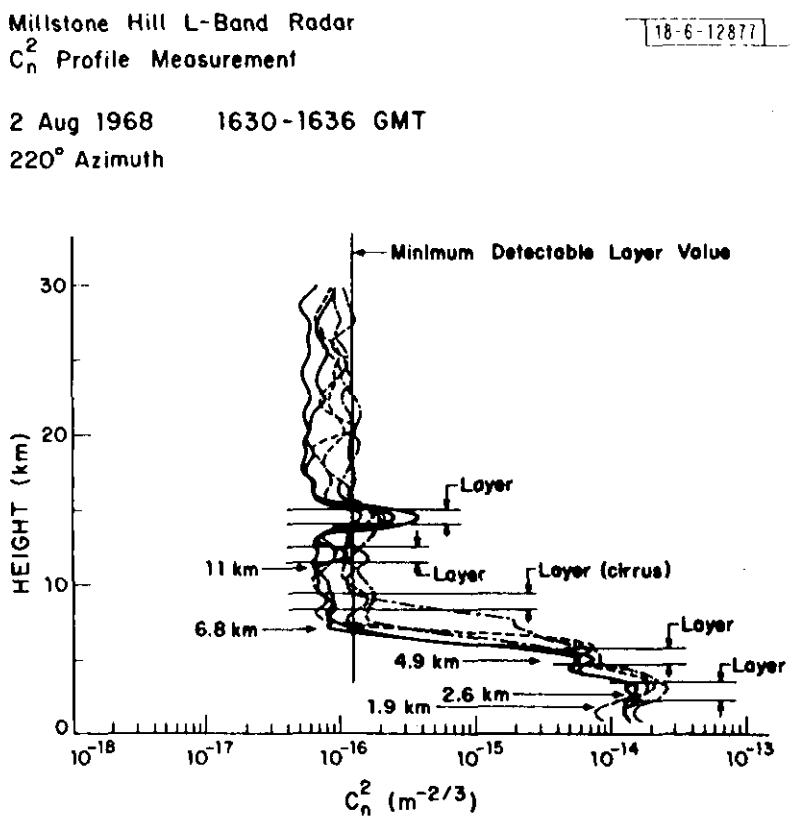

Fig. 2. Weather radar measurement of C_n^2.

scattering from the layer, the radar data may be used directly with the assumption that Δh is given by the height integration distance.

IV. BISTATIC SCATTER MEASUREMENTS

Measurements of transmission loss were made at a frequency of 7.74 GHz using a 145-km scatter path with the transmitter in Avon, Connecticut* and the Westford Communications Terminal as the receiver. The parameters for the scatter path are listed in Table II. Figures 3 and 4 give the geometry of the scatter path. The path cross section, Fig. 4, was generated using a "4/3 earth" model. The scatter path is over the hills of northeastern Connecticut and south central Massachusetts. The hills are all of about the same height and no obstacle is simultaneously visible to both transmitter and receiver. For this path the terrain diffracted signal would arrive after multiple diffractions and is orders of magnitude below the minimum detectable transmission loss value. Further protection against low angle paths is provided at the transmitter location by foliage and solid earth shielding. Along the great circle path, solid earth shielding occurs for elevation angles below 0.5° and foliage shielding at angles below 2.5°. The latter value was used for the transmitter horizon on Fig. 4.

The foreground is shown in Fig. 5. From Fig. 5, it is seen that the minimum shielding angle occurs between 50 and 52° azimuth. Alignment of the transmitter for maximum signal strength would be at 51° azimuth not 48.8° azimuth which corresponds to the great circle path. Transmission loss as a

---

* Site provided courtesy of WTIC, Hartford, Connecticut.

TABLE II

AVON - WESTFORD X-BAND SCATTER PATH PARAMETERS

Frequency	7.74 GHz (3.88 cm wavelength)
Antenna 1	60-foot parabola with Cassegrain feed
Aperture efficiency antenna 1, η	40 percent
Beamwidth antenna 1	0.15° between half-power points
C_{φ}^{2}	1.48
Polarization antenna 1	Left-hand circular received
Antenna 2	6-foot parabola with prime focus feed or standard gain horn
Gain antenna 2	39.5 dB for 6 foot 18.2 dB for horn
Beamwidth antenna 2	1.5° for 6 foot 23° for horn
Polarization antenna 2	Vertical or horizontal linear transmitted
Transmitter power	Variable to 500 w
Transmitted signal	cw with frequency stable to 1 part in 10^{10} per day
Receiver	Phase lock
Receiver bandwidth	500 Hz
Receiver noise temperature	250°K (includes atmosphere and ground effects)
Maximum detectable transmission loss	220 dB with 6 foot 200 dB with horn
Path length	145 km
Data processing	Received signal AGC voltage and local oscillator frequency sampled 20 times per second

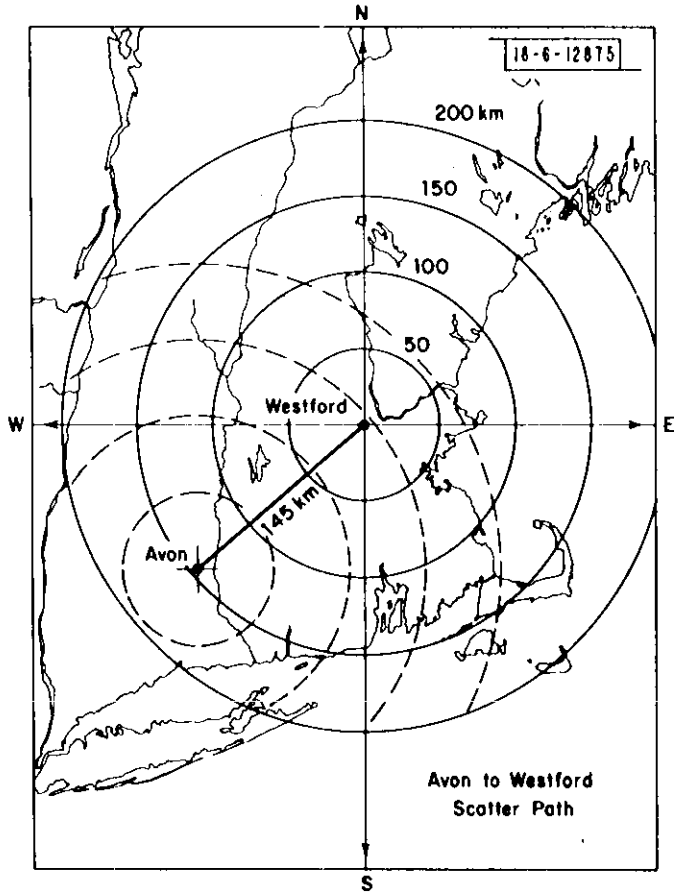

Fig. 3. Avon to Westford scatter path.

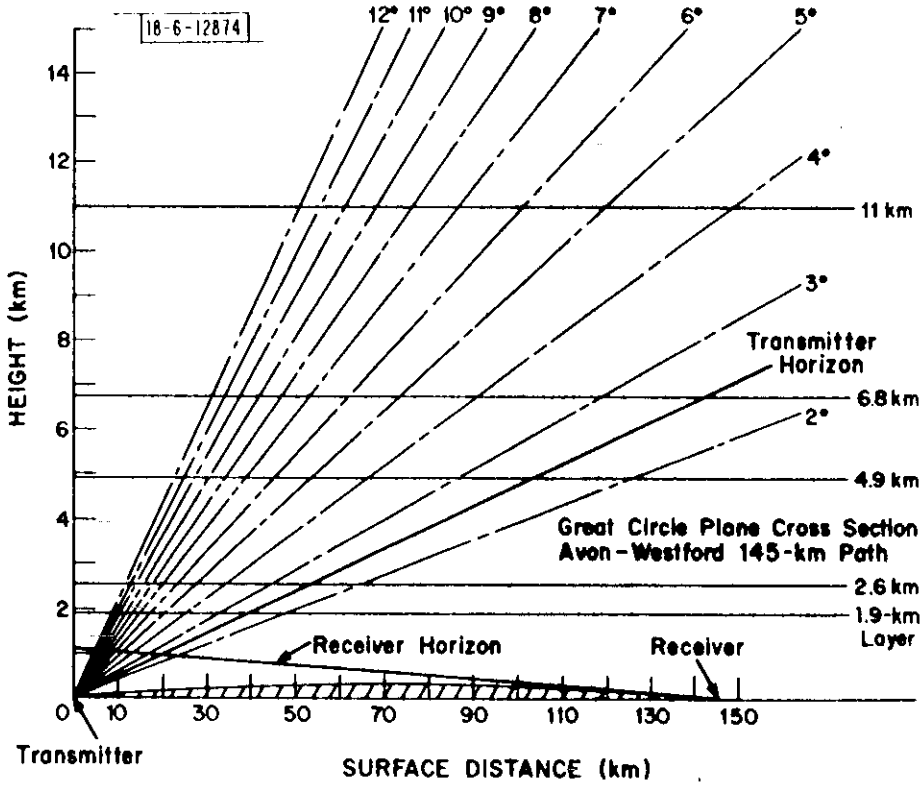

Fig. 4. Great circle plane cross section for Avon to Westford path.

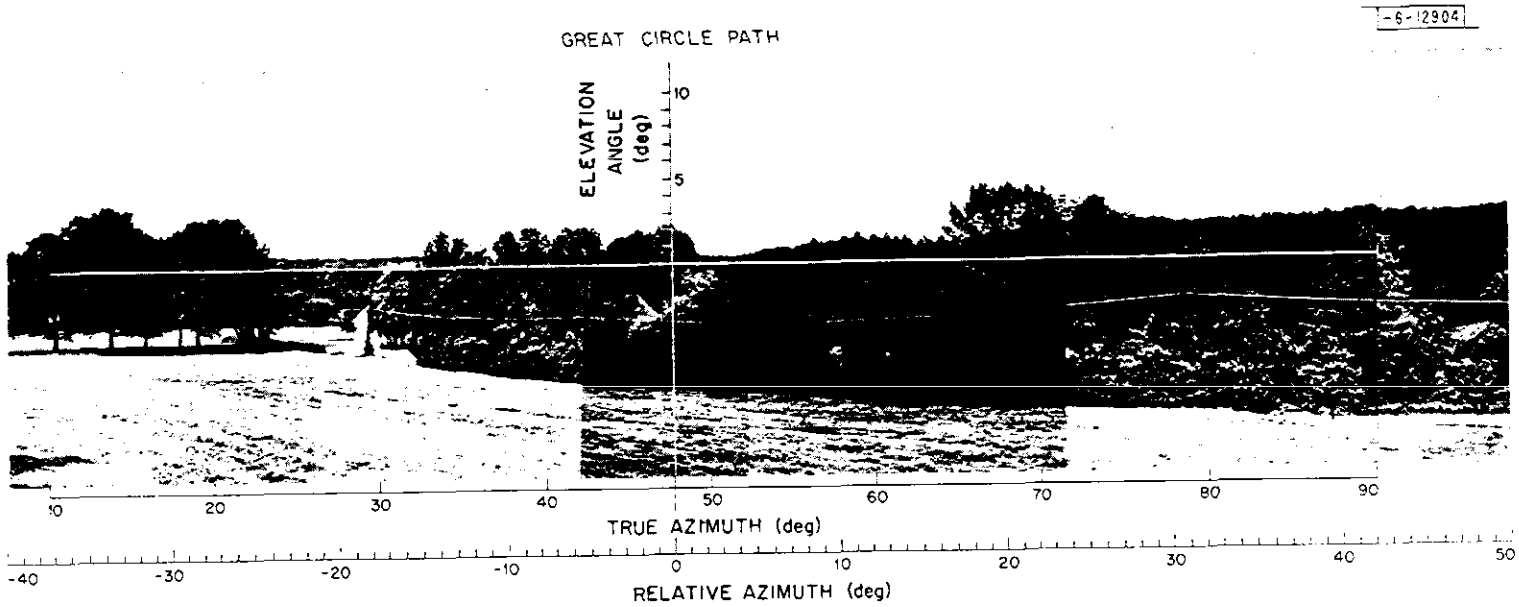

Fig. 5. Foreground at Avon, Connecticut.

function of receive antenna azimuth angle is shown in Fig. 6. The data was taken by slowly scanning the 60-foot receive antenna in azimuth at a fixed 1° elevation angle about the great circle path (229.5°). The data points represent 1-second averages of received power and receiver pointing angle and the lines represent 10-second averages. The uncertainty in the calibration of the bi-static scatter system yields an uncertainty of 0.2 dB in the measured transmission loss. The 6-foot transmit antenna was positioned at 1° elevation and 48.8° azimuth. At these angles, the half-power beamwidth of the antenna intersected the trees and the transmission loss along the great circle path was 22 dB greater than for the same receive antenna pointing angles and the transmit antenna elevated to 4° along the great circle path. At 4°, the half-power beamwidth clears the trees. Some of the changes in transmission loss may be due to the scattering layer structure in the lower 2 km of the atmosphere but the primary effect is attenuation due to foliage shielding. The azimuthal dependence of the received signal as shown on Fig. 6 also supports the hypothesis. The signal is maximized not along the great circle route, but to the south, in the direction for which the illumination of the scattering layers would be strongest due to the lower shielding angles between 50 and 52° azimuth at Avon.

Both the intensity and doppler shift of the received signal were recorded. Figure 7 shows the doppler shift vs azimuth measurements taken at the same time as the intensity measurements shown in Fig. 6. For scattering by thin layers, the scatterers move with the wind at the height of the layer. The

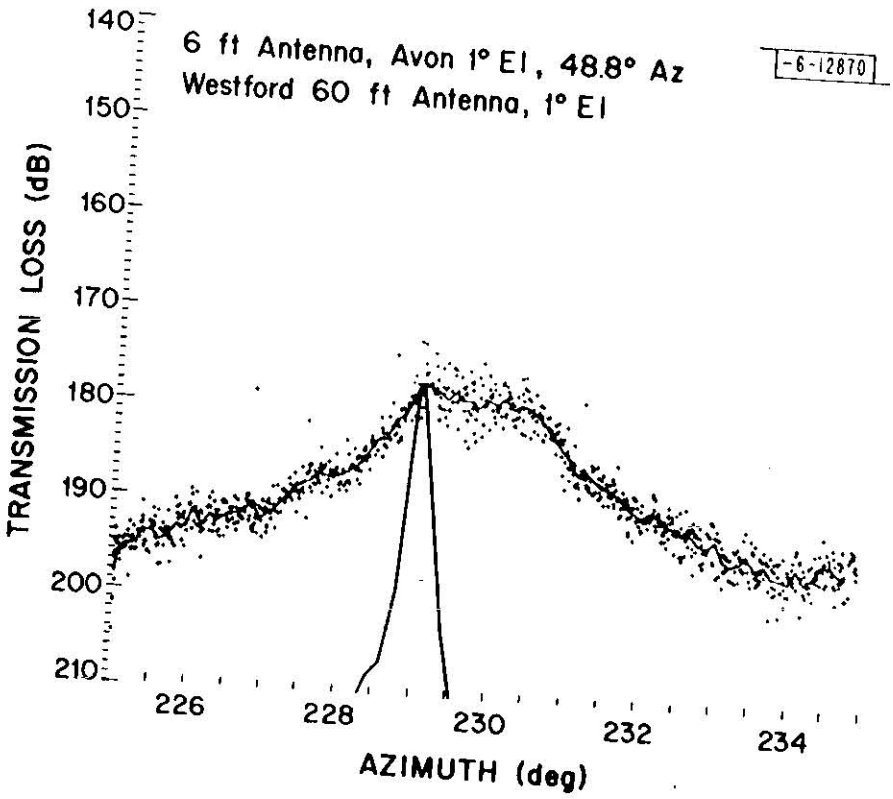

Fig. 6. Transmission loss vs receive antenna azimuth.

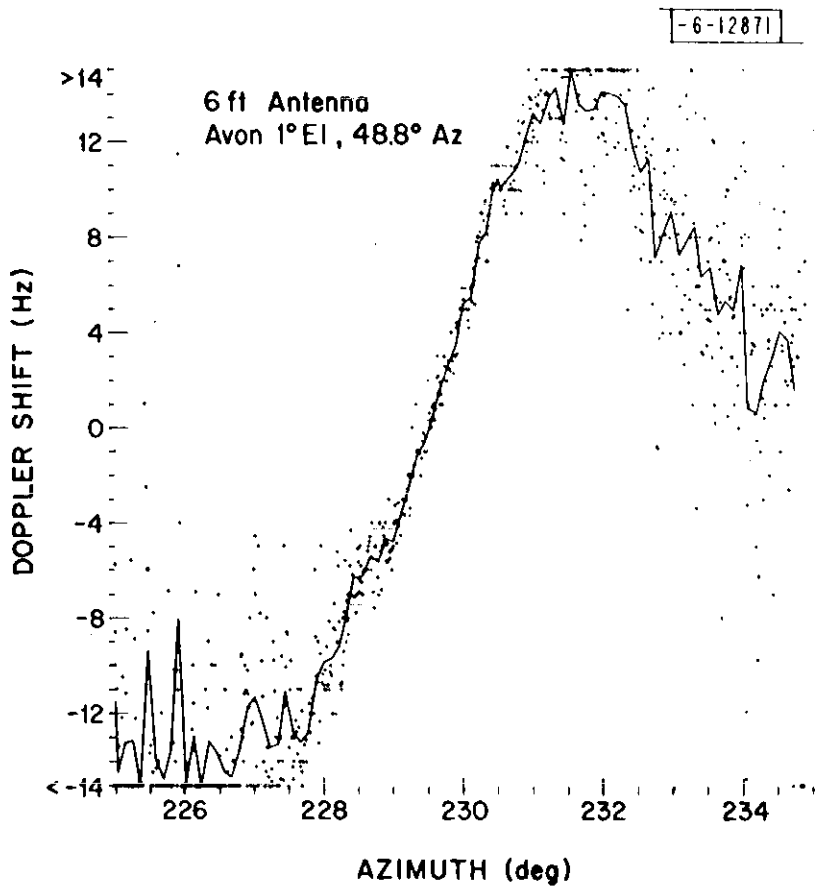

Fig. 7. Doppler shift vs receive antenna azimuth.

motion is predominantly horizontal hense the doppler shift should be zero along the great circle path and be negative or positive off the path as dictated by the horizontal wind. Equation (13) for scattering by thin turbulent layers indicates that as the scattering volume is moved away from the great circle plane, the scattering angle increases and the transmission loss rapidly increases. With increasing transmission loss, the point is reached where the strongest signal is received through the side lobes of the 60-foot antenna. When the signal is coming from the intersection of the scattering volume and the main lobe of the receiving antenna, the measured doppler shift changes from positive to negative values as shown in Fig. 7 for azimuths between 228 and 232 degrees. As the receive antenna is pointed further away from the direction of maximum signal, the effect of side lobe coupling becomes relatively more important and the magnitude of the doppler shift of the composite signal becomes smaller until, with the signal received through the side lobes, the doppler shift for the peak signal is obtained. The zero reference for doppler shift was taken as the value for the great circle azimuth on Fig. 7. From Fig. 7 it is also seen that the scattering model, Eq. (13) is useful only between 228 and 232 degrees where the signal is received via the main lobe of the receive antenna.

The doppler shift measurements were used to determine when the scattered signals were received via the main lobe and to detect scattering by aircraft. Aircrafts have much larger scattering cross sections than turbulence.

Aircrafts also have doppler shift signatures quite different from the turbulent layers. When scattering from aircraft was present, the data were not included in the analysis. The minimum values of transmission loss detected during the two-week scatter measurement program were all caused by aircraft. The effects of aircraft however are transient.

V. COMPARISONS BETWEEN ESTIMATED AND MEASURED TRANSMISSION LOSS

Simultaneous radar and bistatic scattering measurements of rain and thin turbulent layer scattering were made during a two-week period July 29 - August 9, 1968. During this measurement period 24 hours of rain scatter data and 47 hours of thin turbulent layer scatter data were obtained. The results presented in this section are typical of those obtained during the measurement program. The comparison between radar and bistatic scatter data was made using the model equations developed above. The comparisons are made to establish the validity of the models. The models relate only to the relative minimum in transmission loss that occur when the receiver antenna beam is pointed at the rain cell or layer illuminated by the transmitter.

Rain scattering measurements are shown in Figs. 8 and 9. These measurements were made on two successive azimuth scans of the receive antenna for the same transmit antenna pointing angles. The elevation angle of the receiver was changed between the scans. In both scans, the scattering volumes were below the melting layer. The cells for which model computations were made are marked by vertical arrows. The measurements presented in Fig. 9

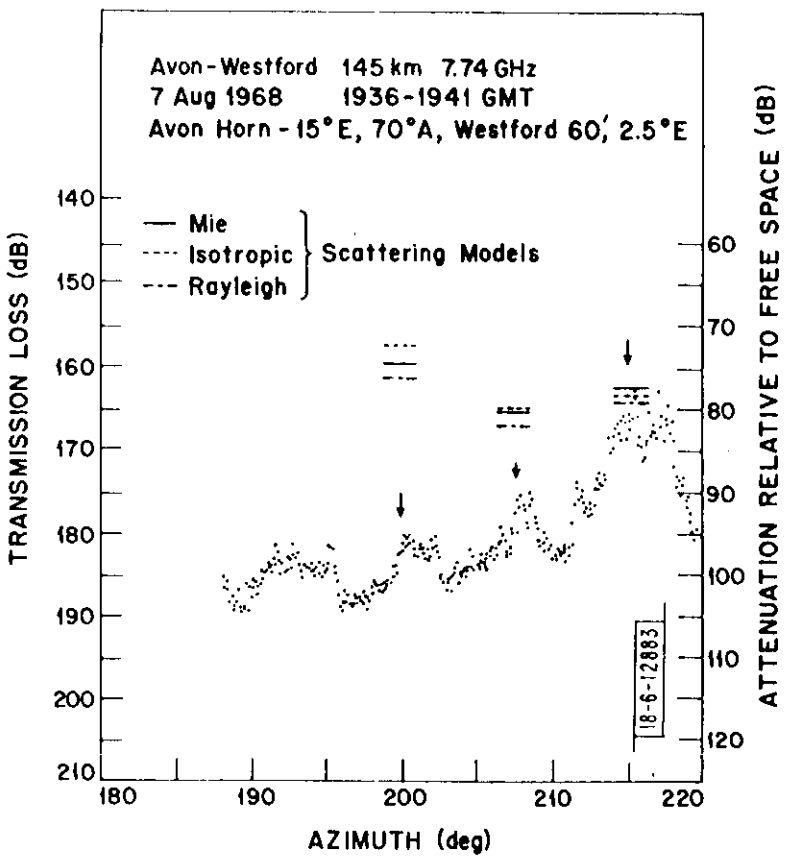

Fig. 8. Transmission loss vs receive antenna azimuth, 2.5° receive elevation angle.

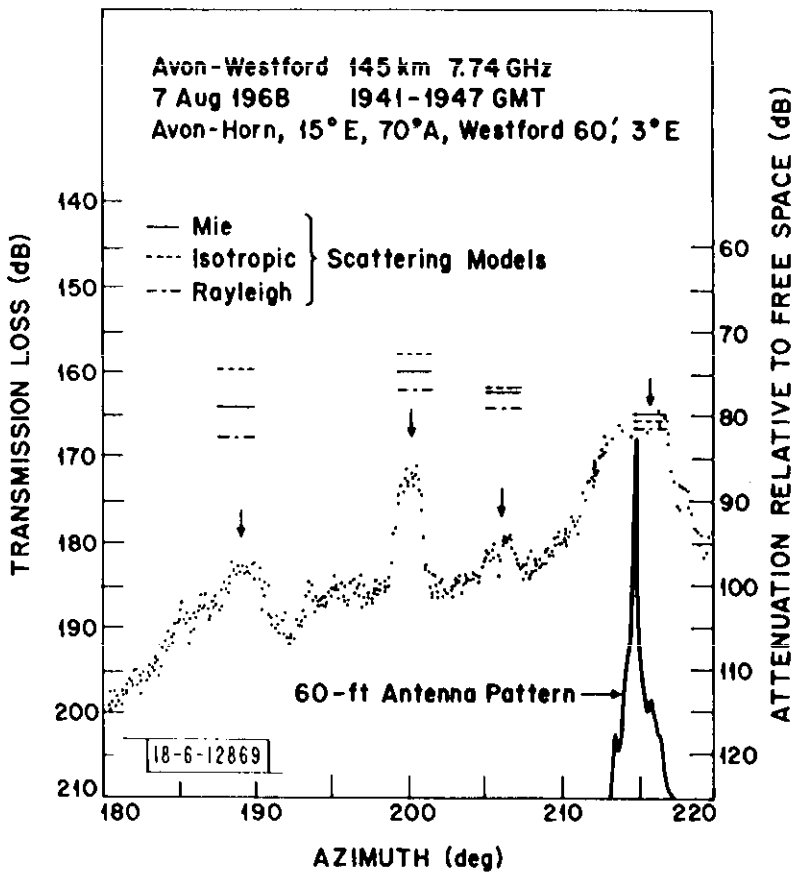

Fig. 9. Transmission loss vs receive antenna azimuth, 3.0° receive elevation angle.

were made simultaneously with the radar measurements presented in Fig. 1. Using the improved rain scatter model, Eq. (12), the scatter path parameters listed in Table II, $C_p = 1/2$ because of the difference in transmitter and receiver polarization and a $|K|^2$ value of 0.93, the results are shown as the horizontal lines. Three sets of computations were made, one based on the isotropic model, one on the Rayleigh model, and one on Mie theory computations and the Laws and Parsons (1943) drop-size distribution. The transmitted polarization was horizontal and for the range of scattering angles used $\alpha_{||}$ was used in the computations. The elevation angles for ray paths between the scatterers and the transmitter varied between 1.7° and 2.3° for both scans. The cell at 215° azimuth was simultaneously visible to both antennas. For each of the other cells, the ray path passed through the trees. More shielding is expected for the measurements presented in Fig. 8 because the scattering volumes were lower. This is evident in a comparison between the estimated and measured values at 200° azimuth.

The cell at 215° azimuth is the only one with no site shielding. The bistatic scattering measurements agree with the estimated value derived from the radar data to within the accuracy of the radar measurements. The maximum value of attenuation due to shielding, the difference between the Mie theory estimate and the measured value was 22 dB which is the same as given above for shielding in the thin turbulent layer measurements. In both cases, the line-of-sight between the transmitter and the scatter volume passed through the trees but not the solid earth.

Doppler shift measurements were also made on the rain scattered signal. The doppler shift measurements made simultaneously with the transmission loss measurements given in Fig. 9 are given in Fig. 10. Evident in this figure is the spatial variability in doppler shift and the requirement for making measurements with a frequency tracking receiver. In some cases, a frequency spread in excess of 500 Hz was observed on an auxiliary spectrum analyzer. In these cases, the measured signal would be lower than that estimated. A large frequency spread was not evident at the time that the measurements of the cell at 215° azimuth were made.

Thin turbulent layer scattering measurements are shown in Figs. 11 and 12. The elevation scan presented in Fig. 11 was made in the great circle plane with the transmit antenna elevated to 2° and looking into the trees. The scan presented in Fig. 12 was made with the transmit antenna elevated to 8°. In both sets of measurements, scattering by thin layers are evident. The arrows in Fig. 12 represent layer heights deduced from the composite of a series of elevation scans with the transmit antenna angle increased by 1° from scan to scan. The data as represented by lines passing through the center of the scatter of 1 second average points is presented in Fig. 13, together with smooth curves that represent the layer heights. The curves for layer heights were computed using a "4/3 earth" geometry and selecting heights that best fit the peaks of the scatter data. From the superimposed antenna pattern, it is seen that the relative minimum in transmission loss are caused by scattering in the

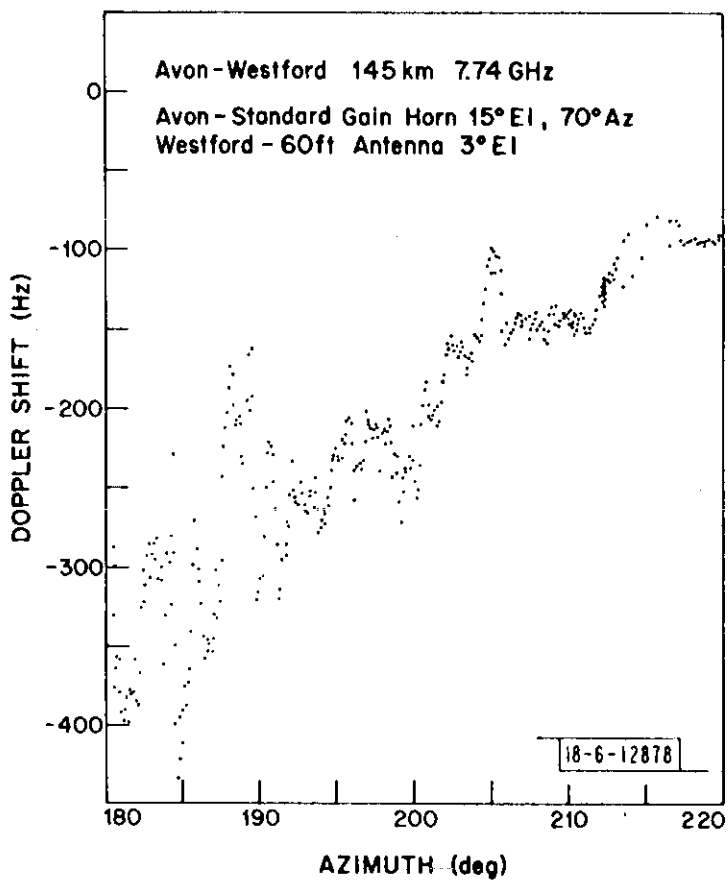

Fig. 10. Doppler shift vs receive antenna azimuth, 3.0° receive elevation angle.

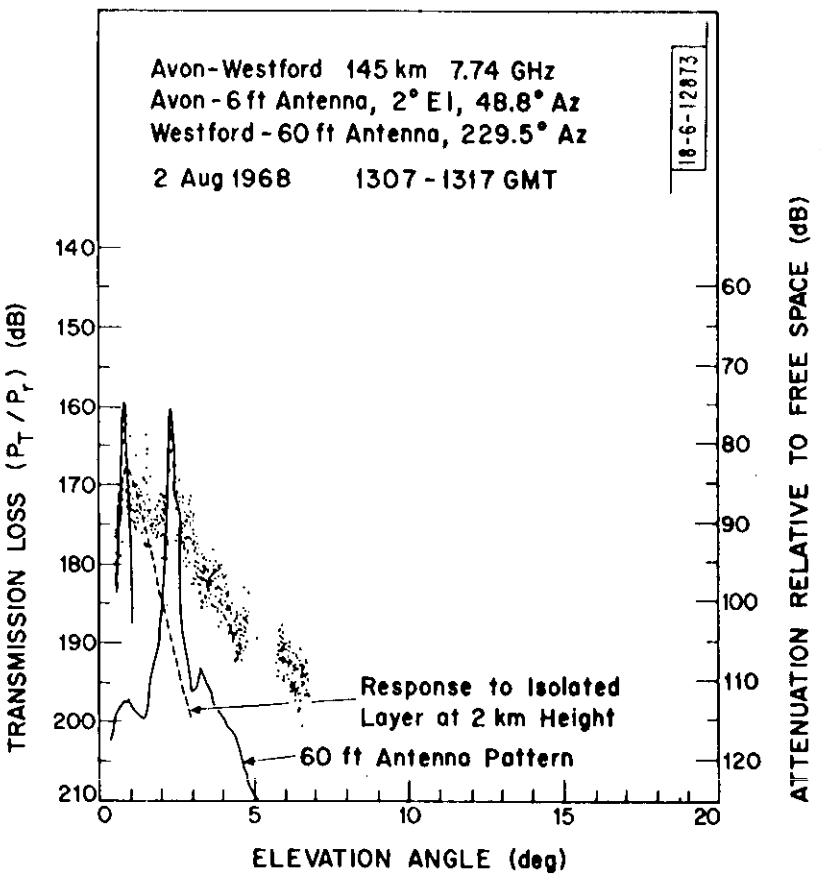

Fig. 11. Transmission loss vs receive elevation angle, 2.0° transmitter elevation angle.

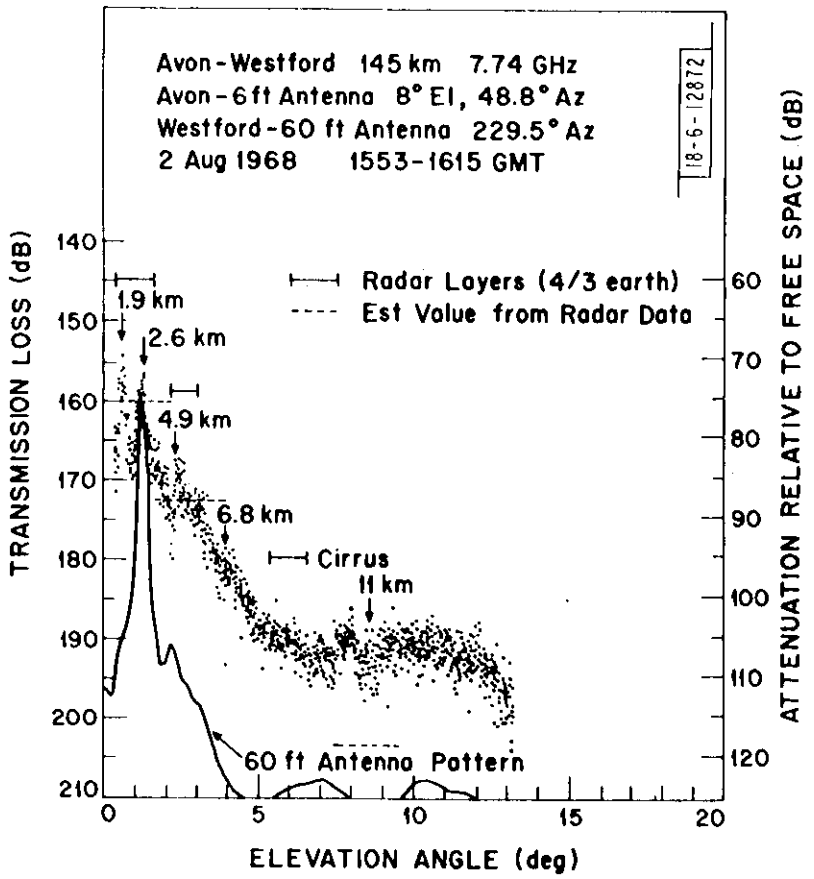

Fig. 12. Transmission loss vs receiver elevation angle, 8.0° transmitter elevation angle.

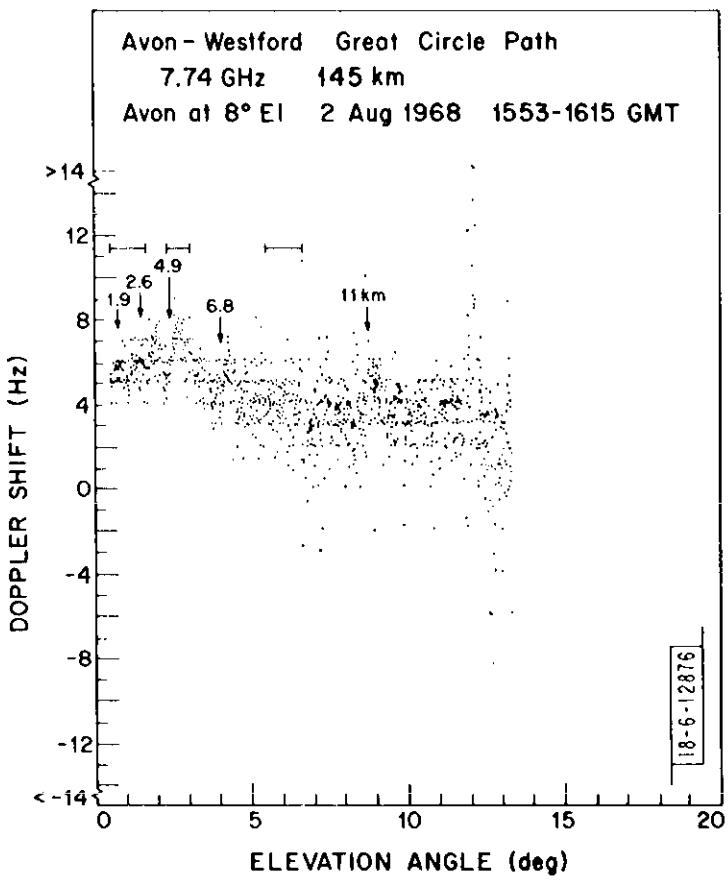

Fig. 13. Doppler shift vs receive elevation angle, 8.0° transmitter elevation angle.

main lobe of the antenna pattern and no single layer plus side lobes dominates the received signal.

The dashed curve superimposed on Fig. 11 represents the expected response to a single layer at 2 km height as given by Eq. (13). From Fig. 2 which gives the $C_n^2 \Delta h$ profile for the measurements shown in Figs. 11-13, it is seen that a broad layer or a series of unresolved layers exist in the 1.5 - 4 km height region. Figure 12 shows layers both at 1.9 and at 2.6 km. If these layers were directly illuminated, the results of the model computation would give the dashed curve, but at a lower transmission loss value. As the transmitter elevation angle increases, the apparent angular width at the receiver over which a layer contributes to the received signal decreases as shown by the measured layers at 1.9 and 2.6 km on Fig. 12. The data on Fig. 11 is for a transmitter elevation angle of 2° which is a condition of partial blockage by trees. If it is assumed that the effect of scattering and absorption by the trees is to attenuate the signals at elevation angles below 2.5° such that only the energy from the side of the main lobe at angles greater than 0.5° from the antenna pointing angle contributes, the result should look like that expected for an elevation angle of 2.5° but with a higher transmission loss. A comparison of transmission losses at 1° and 2° receiver elevation angles for transmitter elevation angles between 2° and 8° shows an increase in transmission loss at the 2° transmitter elevation angle. Computations of the receiver elevation angle dependence from a single layer at 2 km height also show a marked

decrease in effective angular width at a 2.5° elevation angle as is shown by the data.

For a transmitter elevation angle of 8° and layers at 2.6, 4.9, and 11 km the scattering volume is visible to both the transmitter and receiver. Using the $C_n^2 \Delta h$ data given in Fig. 2 and the improved turbulent layer scatter model, the transmission losses indicated by the dashed horizontal lines in Fig. 12 result. Good agreement is obtained for the lower, stronger layers at 2.6 and 4.9 km height. The predicted signal strength for the 11 km layer is much less than measured. Although the side lobe contributions at the elevation angle of the 11 km layer from any one of the strong layers is smaller than the value predicted for the 11 km layer, incoherent addition of energy from all the layers through the side lobes produced a signal level much higher than estimated. Since, in the side lobes, the scattering volume is effectively larger than for reception through the main lobes due to the large horizontal extent of the scattering layers, the side lobe contributions of the strong layers will also be higher than indicated by the superimposed antenna pattern positioned at any of the layer peaks. At the large scattering angle that obtains for the 11 km layer, the model does not hold due to the neglect of the effects of side lobes of the lower, stronger layers.

Doppler shift measurements were also made during the elevation scans. The results for the receiver elevation scan with the transmitter antenna at an 8° elevation angle is given in Fig. 14. As in Fig. 13, the locations of the

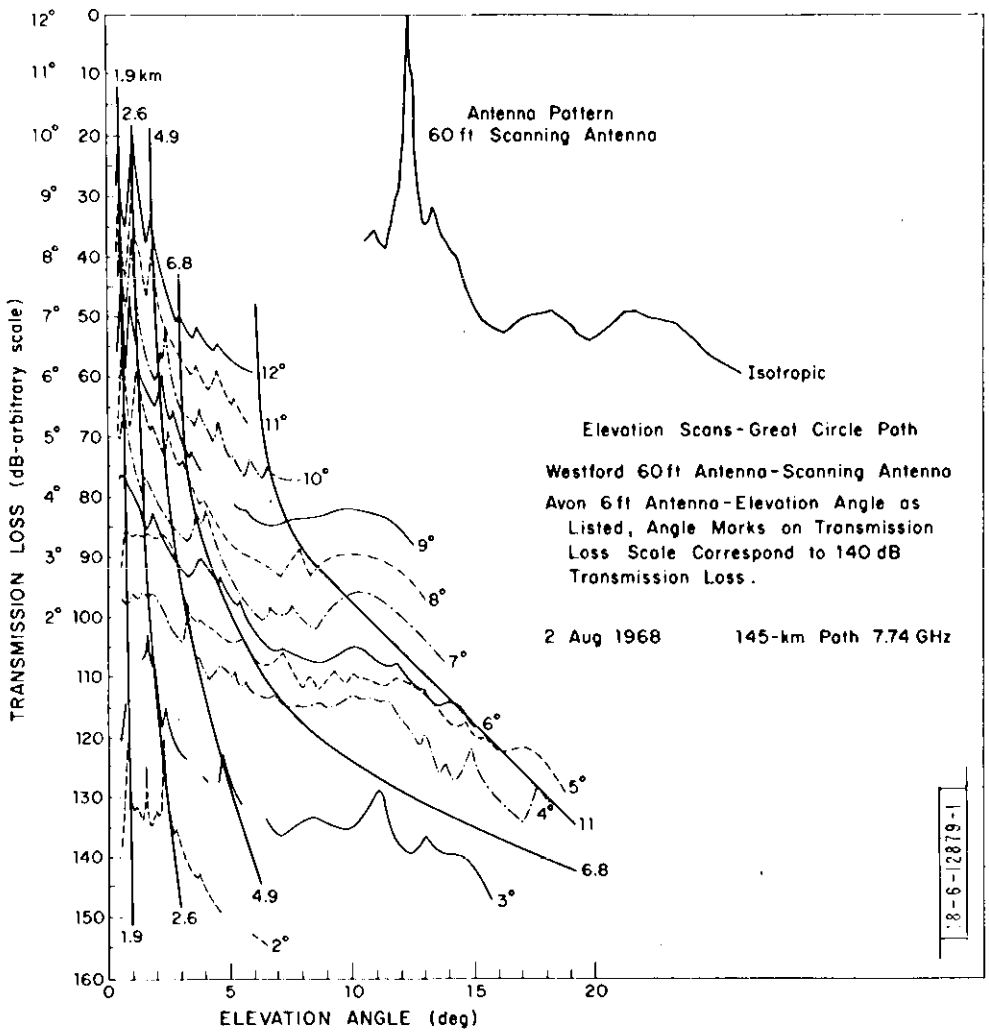

Fig. 14. Transmission loss vs receive elevation angle, 2°-12° transmitter elevation angle.

scattering layers are shown by the vertical arrows and the radar measurements by horizontal bars. It is expected that the doppler shift would be very small for elevation scans in the great circle plane. When compared with the azimuth scan measurement data presented in Fig. 7, the relative shift as a function of elevation angle is small. The zero doppler shift value was selected using the data on Fig. 7. The difference in doppler shift between the data arises from the effect of site shielding on the low elevation angle data. The maximum signal came from off the great circle path in the data of Figs. 6 and 7 used to establish the zero value of doppler shift. The data for the great circle path and no shielding show a more positive value. The increase in the spread of data points with increasing elevation angles occurs because of the decrease of signal-to-noise ratio in the phase lock loop.

VI. SUMMARY OF RESULTS

The comparisons between the radar and bistatic scattering measurements using the improved model equations show agreement within the measurement accuracies of both the radar and bistatic scatter systems. This agreement occurs when no site shielding occurs and the cells or layers are relatively intense. These last two conditions will always be met when interference prediction computations are made. Additional path loss was detected due to foliage along one of the paths indicating that site shielding is an effective method for reducing the strong signals that arrive by low elevation angle paths.

The comparison computations were made using the improved models,

Eqs. (12) and (13). If the simple models, Eqs. (8) and (10) were used, the transmission loss would be 2.7 dB higher for the case of turbulent scatter and 2.4 dB higher for the rain case. For estimations of field strength, the simpler model is with 5 dB of the measured transmission loss value and has the advantage of not requiring the parameters η and C_φ for the antenna.

The angular dependence of the scattering cross sections show that rain is an important source of interference for all scattering angles. Due to the $\left[\sin\left(\frac{\psi_1 + \psi_2}{2}\right)\right]^{-11/3}$ factor, turbulent scattering is important only for a small cone of antenna pointing angles about the horizon angle along the great circle path. Although, in extreme cases, turbulent layer scattering may produce larger signals than rain scatter for scatterers located with the small cone of pointing angles, the measurements shown in Fig. 15 indicate that along the great circle path and with 2.5° site shielding, rain is still more important. From the measurements, the small cone of angles extends to about 5°.

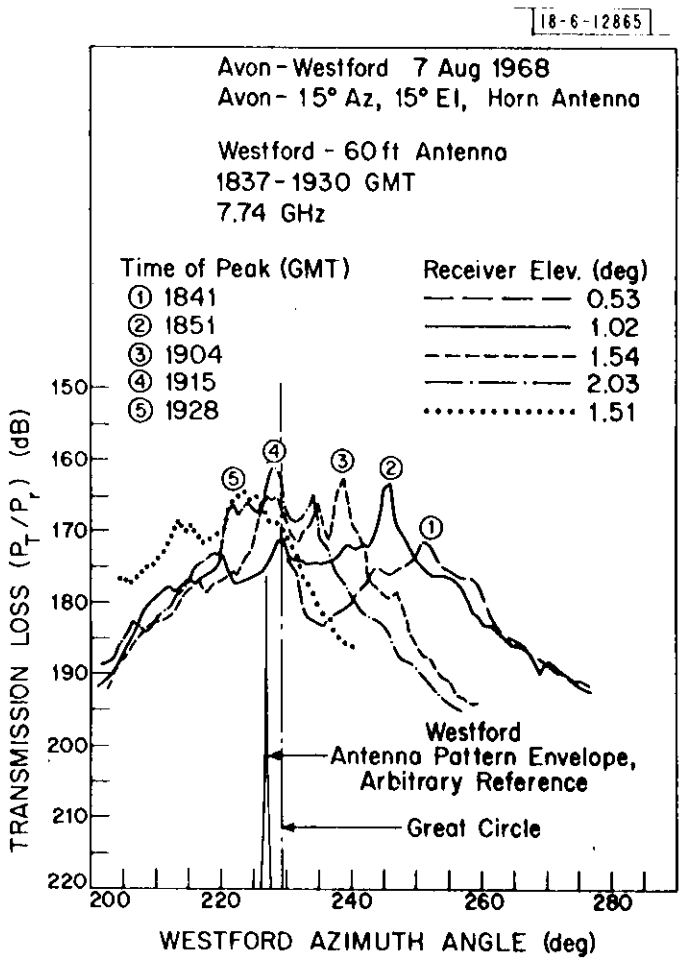

Fig. 15. Transmission loss vs receive antenna azimuth for .5-2° receive antenna elevation angle.

REFERENCES

1. R. K. Crane, "Microwave Scattering Parameters for New England Rain," Technical Report 426, Lincoln Laboratory, M. I. T. (3 October 1966).

2. _____ "Simultaneous Radar and Radiometer Measurements of Rain Shower Structure," Technical Note 1968-33, Lincoln Laboratory, M. I. T. (18 September 1968).

3. _____ "Monostatic and Bistatic Scattering from Thin Turbulent Layers in the Atmosphere," Technical Note 1968-34, Lincoln Laboratory, M. I. T. (18 September 1968).

4. _____ "Measurement of Clear Air Turbulence in the Lower Stratosphere using the Millstone Hill L-band Radar," (to be published in the Proceedings of the 14th Weather Radar Conference, Am. Meteorol. Soc., Boston, 1970).

5. J. O. Laws and D. A. Parsons, "The Relation of Raindrop - Size to Intensity," Am. Geophys. Union Trans. 24 (1943) p. 452.